Bachelor's degree thesis

ANALYTIC STABILITY MAPS OF UNKNOWN EXOPLANET COMPANIONS FOR IMAGING PRIORITIZATION

Carlos Gascón Álvarez

Advised by

Dmitry Savransky (Cornell University)
Miquel Sureda (UPC)

In partial fulfillment of the requirements for the

Bachelor's Degree in Mathematics
Bachelor's Degree in Aerospace Technology Engineering

July 2019

UNIVERSITAT POLITÈCNICA DE CATALUNYA BARCELONATECH
Escola Superior d'Enginyeries Industrial, Aeroespacial i Audiovisual de Terrassa

UNIVERSITAT POLITÈCNICA DE CATALUNYA BARCELONATECH
Centre de Formació Interdisciplinària Superior

UNIVERSITAT POLITÈCNICA DE CATALUNYA BARCELONATECH
Facultat de Matemàtiques i Estadística

Cornell University

ABSTRACT

Identifying which systems are more likely to host an imageable planet can play an important role in the construction of an optimized target list for future direct imaging missions, such as the planned technology demonstration for the Wide Field Infrared Survey Telescope (WFIRST). For single-planet systems, the presence of an already detected exoplanet can severely restrict the target's stable region and should therefore be considered when searching for unknown companions. To do so, we first analyze the performance and robustness of several two-planet stability criteria by comparing them with long-term numerical simulations. We then derive the necessary formulation for the computation of (a, R) analytic stability maps, which can be used in conjunction with depth-of-search grids in order to define the stable-imageable region of a system. The dynamically stable completeness (i.e., the expected number of imageable and stable planets) can then be calculated via convolution with the selected occurrence grid, obtaining a metric that can be directly compared for imaging prioritization. Applying this procedure to all the currently known single-planet systems within a distance of 50 pc, we construct a ranked target list based on the WFIRST CGI's predicted performance and SAG13 occurrence rates.

Keywords— numerical simulations - analytic stability maps - dynamical evolution and stability - direct imaging - exoplanets

CONTENTS

1. INTRODUCTION

Despite indirect detection methods, such as radial velocity or transit photometry, have been the main source of exoplanetary information to date, direct imaging emerges as a challenging but highly desirable technique, providing unique information regarding the atmospheric structure and chemical composition of exoplanets (Konopacky et al., 2013). In this context, space-based direct imaging surveys, such as the Wide-Field Infrared Survey Telescope (WFIRST), will surely enable the expansion and better characterization of the known population of exoplanets. Given the high-cost and complexity of space observatories, a detailed and extensive planning is required in order to ensure the successful development of the mission. In particular, regarding the construction of an optimized target list, it is essential to previously identify which systems are more likely to host an imageable planet. Garrett et al. (2017) addressed this problem by defining the depth-of-search grids in the (a, R) space, where the value of each bin represented the probability of detecting a planet with semi-major axis a and radius R. The resultant imageable region was obtained according only to the instrument's performance and capabilities, allowing for the estimation of the expected number of detected planets (i.e., total completeness) by convolution with the desired grid of occurrence rates.

When searching for additional exoplanets in already known single-planet systems, however, the gravitational effect of the existing body can severely restrict the target's stable region and must therefore be taken into account. For instance, let us consider a nearby star with a large imageable region and a massive highly eccentric planet in the center of such region. In this context, most of the detectable area would be chaotic due to the known planet's presence, consequently reducing the probability of detecting a stable unknown companion in a system which a priori seemed a valuable target. In general, for any system the following question is naturally raised: How many stable unknown companions will an instrument detect? We seek to answer this question in an accurate but computationally inexpensive manner, in order to rapidly identify which targets have a higher probability of hosting an additional planet and discard those systems where no unknown companions can be detected. To do so, in Section 2 we begin by describing several two-planet stability criteria and comparing them with long-term numerical simulations. In Section 3 we derive the necessary expressions for the conditional density function of the outer pericenter to inner apocenter ratio (ρ) and the angular momentum deficit (C), which will be essential for the computation of analytic stability maps presented in Section 4. Finally, in Section 5 we make use of this results, together with depth-of-search and occurrence grids, in order to obtain the expected number of imageable and stable planets of a certain target. We conclude by presenting a 189 single-planet systems ranking according to the WFIRST CGI's predicted performance and the SAG13 occurrence rates.

2. ANALYTIC STABILITY CRITERIA FOR TWO-PLANET SYSTEMS

Unlike systems with three or more planets, the stability of two-planet systems can be analytically characterized via several different criteria. One of the main results was obtained by Marchal and Bozis (1982), who extended the notion of Hill stability to the general three-body problem and showed that certain initial conditions can preclude close encounters between the outer planet and the inner bodies. Based on this result, Gladman (1993) found that two planets in initially circular and coplanar orbits are Hill stable if

$$a_2 - a_1 > 2\sqrt{3} R_H \,, \tag{1}$$

where

$$R_H = \left(\frac{m_1 + m_2}{3 M_\star} \right)^{1/3} \frac{a_1 + a_2}{2} \tag{2}$$

is the mutual Hill radius, $M_\star$ is the mass of the central star, a_i are the semi-major axes of the planet orbits, m_i are the planetary masses, and the subscripts 1 and 2 refer to the inner and outer planet, respectively. We shall remember that long-term interactions between planets in Hill stable orbits could ultimately lead to the ejection of the outer planet or the collision of the inner planet with the star (i.e., Lagrange instability). From another perspective, Wisdom (1980) applied the resonance overlap criterion to the coplanar and circular restricted three body problem. By studying the region around a planet where first order mean motion resonances (MMRs) overlap, the author found that a test particle with semi-major axis a would experience chaotic motion if

$$\frac{|a - a_p|}{a_p} < C_{\rm w} \mu_p^{2/7} \,, \tag{3}$$

where $C_{\rm w}$ is a constant value, a_p is the semi-major axis of the planet and $\mu_p = m_p / M_\star$ is the mass ratio between the planet and the star. Although originally Wisdom obtained a theoretical value of $C_{\rm w} = 1.33$, Duncan et al. (1989) presented a numerically-derived estimate of $C_{\rm d} = 1.57$. For the case of two massive planets in circular orbits, Deck et al. (2013) extended Wisdom's criterion and predicted that all orbits should be chaotic if

$$\frac{a_2 - a_1}{a_1} < 1.46 \epsilon^{2/7} \,, \tag{4}$$

where $\epsilon = (m_1 + m_2)/M_\star$ is the planets-to-star mass ratio. Deck et al. (2013) also developed a similar expression for non-circular configurations, only applicable, however, to high-eccentricity orbits. For arbitrary eccentricities, several criteria have been proposed (Giuppone et al., 2013; Petrovich, 2015; Laskar and Petit, 2017; Petit et al., 2017, 2018), which we will divide into two generic categories depending on whether the criterion is based on the outer pericenter to inner apocenter ratio (ρ) or the angular momentum deficit (AMD).

2.1. *Criteria Based on the Outer Pericenter to Inner Apocenter Ratio*

As demonstrated by Petrovich (2015), most of the proposed two-planet stability criteria for arbitrary eccentricities can be expressed as a boundary of the ratio between the pericenter of the outer planet and the apocenter of the inner planet, here denoted by

$$\rho = \frac{a_2(1 - e_2)}{a_1(1 + e_1)} \,, \tag{5}$$

where e_1 and e_2 are the corresponding eccentricities. For instance, Giuppone et al. (2013) developed an extended crossing orbit criterion by adding and subtracting Wisdom's overlap region (Wisdom, 1980, Equation 3) to the outer pericentric and inner apocentric distances, respectively. They also took into account the effect of the difference in the longitudes of the pericenter $\Delta\bar{\omega}$ and proposed stability limits for the case of aligned ($\Delta\bar{\omega} = 0^\circ$) and anti-aligned ($\Delta\bar{\omega} = 180^\circ$) initial orbits. By studying the stability limits of a test planet around a known and existing planet, they presented the following criterion for the anti-aligned configuration

$$\rho > \begin{cases} \dfrac{1}{1 - \delta} & a_2 = a_k \\ 1 + \delta & a_1 = a_k \,, \end{cases} \tag{6}$$

where a_k is the known planet's semi-major axis and $\delta = 1.57(\mu_1^{2/7} + \mu_2^{2/7})$. Here we will make use of the modification proposed by Hadden and Lithwick (2018), where they employ $\delta = 1.46\epsilon^{2/7}$ in accordance to the results of Deck et al. (2013).

Alternatively, Petrovich (2015) approached the problem numerically by performing long-term integrations for a large number of planetary systems and a wide range of eccentricities and inclinations. They found ρ to be the single parameter that best described the stability boundary and presented the following empirical criterion

$$\rho > 1.15 + 2.4\left[\max(\mu_1, \mu_2)^{1/3}\right]\left(\frac{a_2}{a_1}\right)^{1/2}. \tag{7}$$

2.2. *Criteria Based on the Angular Momentum Deficit*

Considering the secular approximation of a planetary system, Laskar and Petit (2017) developed an alternative stability criterion based on the conservation of the angular momentum deficit (AMD). Following the definition of Laskar (2000), the AMD (C) is given by the difference between the norm of the angular momentum of an equivalent circular and coplanar system and the norm of the real system's angular momentum, which for a system of n_p planets is

$$C = \sum_{j=1}^{n_p} \Lambda_j (1 - \sqrt{1 - e_j^2}\cos i_j), \tag{8}$$

where i_j is the relative inclination, $\Lambda_j = m_j\sqrt{GM_\star a_j}$ and G is the gravitational constant. For a two-planet system, Laskar and Petit (2017) defined the relative angular momentum deficit as

$$\mathscr{C} = \frac{C}{\Lambda_2} = \gamma\sqrt{\alpha}(1 - \sqrt{1 - e_1^2}\cos i_1) + (1 - \sqrt{1 - e_2^2}\cos i_2), \tag{9}$$

where $\alpha = a_1/a_2$ represents the semi-major axis ratio and $\gamma = m_1/m_2$ is the mass ratio. In this context, they obtained the minimum relative AMD which allowed for planetary collisions, referred to as the collisional critical AMD $\left(C_c^{\mathrm{C}}\right)$. Consequently, since the AMD is conserved at all orders (Laskar and Petit, 2017), the impossibility of collisions between the two planets is ensured if the initial relative AMD is bounded as

$$\mathscr{C} < C_c^{\mathrm{C}}(\alpha, \gamma). \tag{10}$$

This condition can be extended to multiple planet systems by analyzing the AMD-stability of every pair of adjacent planets, as well as the innermost planet and the star. Furthermore, Agnew et al. (2018) compared the previous criterion with numerical simulations over a large number of known systems and concluded that the AMD-stability is a reliable tool for determining the stability of planetary systems. In order to take into account the effect of mean motion resonances (MMR) ignored by the secular theory, Petit et al. (2017) proposed a new derivation of the first-order MMR overlap criterion in the AMD framework. They refined the criteria presented by Wisdom (1980) and Deck et al. (2013) by deriving a more global expression, for which they then associated a new critical AMD $\left(C_c^{\mathrm{MMR}}\right)$. Since it only makes sense to apply the first-order MMR criterion when α is close to 1, they combined this with the previous collision criterion $\left(C_c^{\mathrm{C}}\right)$ and defined the following piece-wise critical AMD (Petit et al., 2017)

$$\mathscr{C} < C_c(\alpha, \gamma, \epsilon) = \begin{cases} C_c^{\mathrm{C}}(\alpha, \gamma) & \alpha < \alpha_R(\epsilon, \gamma) \\ C_c^{\mathrm{MMR}}(\alpha, \gamma, \epsilon) & \alpha > \alpha_R(\epsilon, \gamma), \end{cases} \tag{11}$$

where α_R represents the semi-major axis ratio at which $C_c^{\mathrm{C}} = C_c^{\mathrm{MMR}}$. For lower values of α, the collisional criterion becomes stricter and consequently more convenient.

Continuing their work in the AMD framework, Petit et al. (2018) generalized the stability criterion proposed by Gladman (1993) and defined the Hill stability AMD criterion

$$\mathscr{C} < C_c^{\mathrm{H}}(\alpha, \gamma, \epsilon) = \gamma\sqrt{\alpha} + 1 - (1+\gamma)^{3/2}\sqrt{\frac{\alpha}{\gamma + \alpha}\left(1 + \frac{3^{4/3}\epsilon^{2/3}\gamma}{(1+\gamma)^2}\right)}, \tag{12}$$

where C_c^{H} is defined as the Hill critical AMD. As this expression was obtained as an approximation of the criterion from Marchal and Bozis (1982), Petit et al. (2018) compared both criteria and proved that Equation (12) is accurate for the typical range of values of ϵ and still valid for very large or small planetary mass ratios (γ).

Table 1. Stellar and Planetary Parameters

Target Star			Known Planet				(a, e) map			(a, m) map		
System	Distance (pc)	$M_\star$ ($M_\odot$)	a_k (AU)	e_k	$m_k \sin I$ (M_J)	ω_k (°)	a (AU)	e	m (M_J)	a (AU)	e	m (M_J)
HD 154345	18.29	0.71	4.21	0.04	0.82	0[a]	[2, 12]	[0, 0.5]	0.1	[1.5, 25]	0.05	[0.067, 134.45]
HD 114613	20.30	1.27	5.34	0.46	0.36	196	[1.5, 20]	[0, 0.5]	1	[1.5, 25]	0.1	[0.067, 134.45]

[a] The argument of periapsis w_k of the planet HD 154345 b was unknown and consequently set to zero.

NOTE.— The (a, m) grid was ranged taking into account the imageable region of each system, which was supposed to be approximately the same in both cases. In particular, the limit values of m approximately correspond to a planetary radius R between 4 and 17 $R_\oplus$.

2.3. *Numerical Simulations and Criteria Comparison*

To assess the performance and robustness of the criteria described above, we performed several numerical simulations in order to study and compare their behaviour over a wide range of parameters. Specifically, we added a test planet to two known single-planet systems (HD 154345 and HD 114613) and analyzed the long-term stability of the resultant two-planet systems. The stellar parameters and the orbital elements of the known planet, denoted by the subscript k, were extracted from the NASA Exoplanet Archive[1] and can be found summarized in Table 1. For simplicity, all systems were assumed to be coplanar and the existing planet's mass was considered to be the minimum value $m_k \sin I$, where I is the system's inclination with respect to the line of sight. The remaining unknown parameters, such as the longitude of the ascending node or the initial mean anomaly, were all set to zero. For each system, we then constructed two different types of stability maps.

1. *(a, e) stability map:* regular grid with 70 logarithmically spaced semi-major axis bins and 40 linearly spaced eccentricity bins. The ranges of a and e were selected taking into the account the extension of the chaotic region around the known planet's semi-major axis a_k. The test planet's mass m was constant through the whole grid, being fixed in a different value depending on the system. In particular, for the system HD 114613 a Jupiter mass planet was added, while a smaller value was used in the case of HD 154345. On the other hand, the argument of periastron $\omega \in [0, 2\pi]$ was always randomly generated.

2. *(a, m) stability map:* regular grid with 70 semi-major axis bins and 40 mass bins, both logarithmically spaced. The range of values of a and m was determined considering the imageable region of the system with the WFIRST CGI. In this case, the test planet's eccentricity e was constant through the whole grid, being fixed in a different value depending on the system. In the case of the system HD 154345, a nearly circular value was used, while a higher eccentricity was asigned to the test planet in the system HD 114613. Finally, ω was again randomly generated.

The particular values employed for every system and stability map are presented in Table 1. For each bin, we integrated the corresponding two-planet system using the Leapfrog integrator implemented in the REBOUND package (Rein and Liu, 2012). The simulations were run for 10^9 yr with a timestep of $T_1/50$, where T_1 is the orbital period of the innermost planet. Integrations were terminated if the two planets approached one another within one mutual Hill radius (Equation 2), or if a planet reached an astrocentric distance of either 5×10^{-3} or 250 AU. The code used to perform the numerical simulations is publicly available at `https://github.com/CarlosGascon/NumSim`.

Figure 1 shows the resultant stability maps for a nearly circular configuration (HD 154345) and a highly eccentric system (HD 114613). In general, we observe that Petrovich's criterion shows the most conservative boundaries, appearing to be too pessimistic in the first case and slightly more appropriate for large eccentricities. In contrast, the complete AMD stability limit (Equation 11) falls inside the chaotic region in most cases and will be consequently discarded for the purposes of the following sections. Similarly to Giuppone's criterion, the Hill AMD boundaries offer an acceptable necessary condition for stability and could therefore be used as a more optimistic alternative. In particular, we remark how the Hill AMD stability condition accurately delimits the earliest chaotic orbits in both (a, e) maps, likely corresponding to the region where planetary close encounters occur. Hence, the remaining instabilities outside these boundaries may be the result of ejections or collisions between the inner planet and the star, which by definition aren't taken into account in the Hill criterion.

Furthermore, the HD 114613 (a, m) stability map shows a pronounced increase in the Hill stability limits as the test planet's mass decreases, disagreeing with other criteria and the numerical simulations. Such behavior becomes more significant for high eccentricities and can be related to the Hill stability's strong dependence on the planetary mass ratio γ for non-circular configurations (Deck et al., 2013). We must keep in mind that the Hill

[1] The required orbital parameters where retrieved from the NASA Exoplanet Archive (https://exoplanetarchive.ipac.caltech.edu) on 2019 June 8.

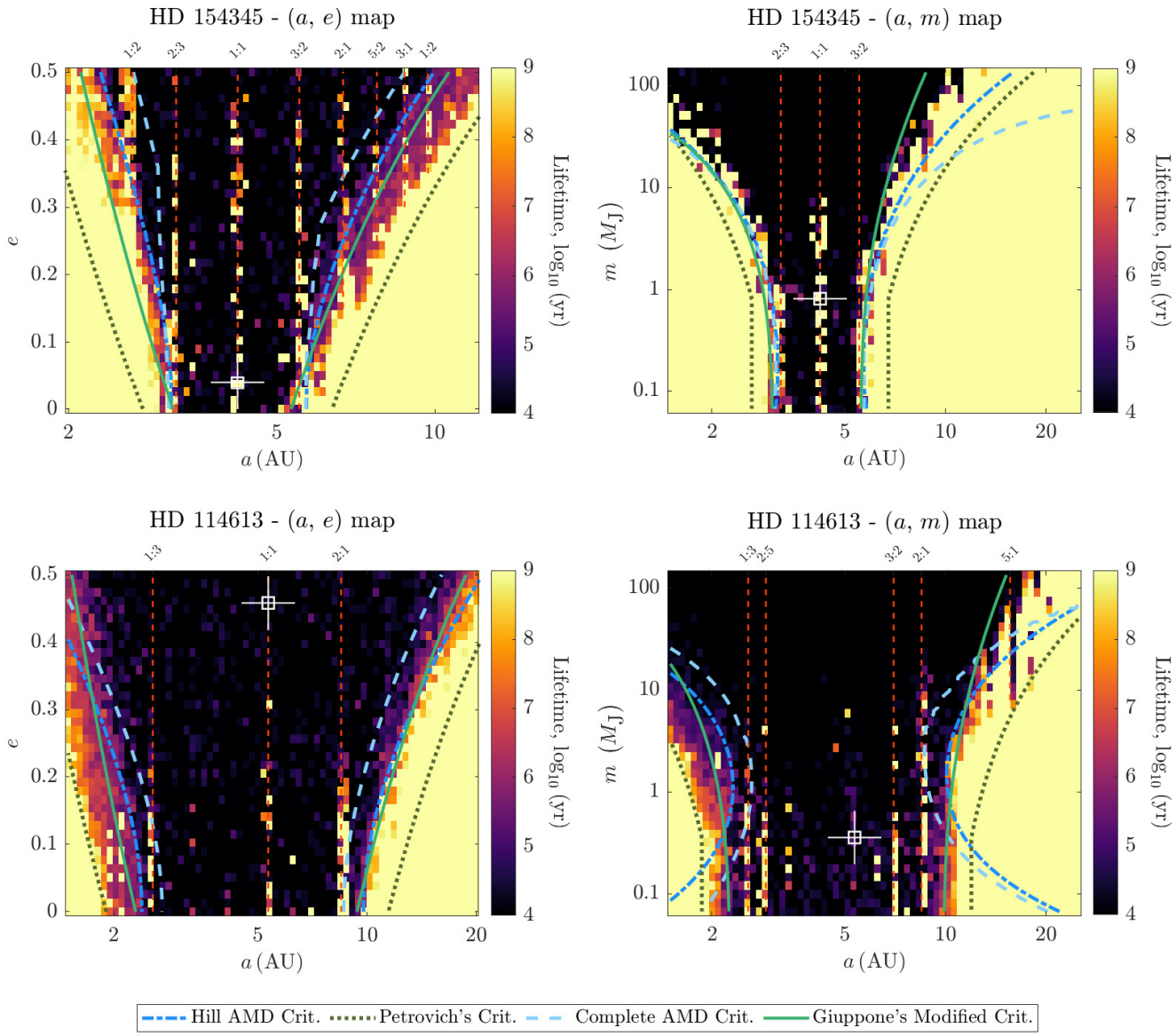

Figure 1. Numerical stability maps for the nearly circular system HD 154345 (top) and high eccentricity system HD 114613 (bottom), compared to the stability boundaries given by the criteria specified in the legend. The white marker indicates the position of the existing planet and the red dashed lines indicate low-order mean motions resonances with the known planet.

stability criterion from Marchal and Bozis (1982) cannot be directly applied to the elliptic restricted three body problem and therefore shouldn't be used when one of the planetary masses is close to zero. Nonetheless, given that in most cases the WFIRST-imageable region only covers high-mass planets, the Hill AMD can still be considered a valid criterion in the following sections. Regarding the test planet's mean motion resonances with the existing planet, we note how for the nearly circular case, the stable resonant lines are more predominant and extend up to larger values of e and m, while being less numerous and significant in the high-eccentricity system.

3. DERIVATIONS

Let us consider a coplanar, three-body system consisting of a central star of mass $M_\star$, and two orbiting planets, where the mass and orbital elements of one of the planets (a_k, e_k, m_k) are known. The remaining planet is unknown, and its parameters (a, e and m) will be consequently treated as random variables. In particular, the eccentricity e will follow a Rayleigh distribution with parameter σ (i.e. mean eccentricity $\mu_e = \sigma\sqrt{\pi/2}$), while the semi-major axis a and the planet's mass m will have a joint probability density function $f_{\bar{a},\bar{m}}(a, m)$ representative of the population of interest. With this setup, for fixed values of a and m, the integral of the conditional density function of both the AMD (C) and the outer pericenter and inner pericenter ratio (ρ) can be easily solved. As will be shown in Section 4, this result will be essential for the computation of the analytic stability maps and the prioritization of planetary systems for followup imaging.

3.1. ρ *Conditional Density Function*

Making use of Equation (5), the outer pericenter to inner apocenter ratio can be rewritten as

$$\rho = g_\rho(e, a) = \begin{cases} \dfrac{q_k}{a(1+e)} & a < a_k \\ \dfrac{a(1-e)}{Q_k} & a > a_k \,, \end{cases} \tag{13}$$

where $q_k = a_k(1 - e_k)$ and $Q_k = a_k(1 + e_k)$ are, respectively, the known planet's pericenter and apocenter. For a fixed semi-major axis a, we observe that $\rho = g_\rho(e \mid a)$ is a univariate function only dependent on e. Consequently, the inverse function $h_\rho = g_\rho^{-1}(\rho \mid a)$ is directly obtained by isolating the eccentricity in Equation (13)

$$e = h_\rho(\rho \mid a) = \begin{cases} \dfrac{q_k - a\rho}{a\rho} & a < a_k \\ \dfrac{a - Q_k\rho}{a} & a > a_k \,. \end{cases} \tag{14}$$

For simplicity, we will omit the conditional notation in $h_\rho(\rho)$ from here on out, since we are primarily interested in evaluating all expressions for a given value of a. Taking the derivative of Equation (14) with respect to ρ, we get

$$\left|\frac{dh_\rho}{d\rho}(\rho)\right| = \begin{cases} \dfrac{q_k}{a\rho^2} & a < a_k \\ \dfrac{Q_k}{a} & a > a_k \,. \end{cases} \tag{15}$$

Using Equations (14) and (15), the ρ conditional density function is then given by

$$f_{\bar{\rho}|\bar{a}}(\rho \mid a) = f_{\bar{e}}(h_\rho(\rho)) \left|\frac{dh_\rho}{d\rho}(\rho)\right| \,, \tag{16}$$

where $f_{\bar{e}}(e)$ is the density function of the eccentricity, assumed to be Rayleigh distributed. For fixed values of a and m, the probability of having a stable configuration, denoted by $S_\rho(a, m)$, is obtained by integrating Equation (16) over the region defined by the specific ρ stability criterion used:

$$S_\rho(a, m) = \int_{\rho_{c,l}}^{\rho_{c,u}} f_{\bar{\rho}|\bar{a}}(\rho \mid a) d\rho = F_{\bar{e}}(h_\rho(\rho_{c,u})) - F_{\bar{e}}(h_\rho(\rho_{c,l})) \,, \tag{17}$$

where $\rho_{c,l}(a, m)$ and $\rho_{c,u}(a, m)$ are the lower and upper limit respectively. Given our assumptions, the integral can be simply calculated as the difference between the Rayleigh cumulative distribution function $F_{\bar{e}}(e)$ evaluated at the limiting eccentricities $h_\rho(\rho_{c,u})$ and $h_\rho(\rho_{c,l})$. Substituting h_ρ from Equation (14) yields the analytic solution

$$S_\rho(a, m) = \begin{cases} -\exp\left(\dfrac{-1}{2\sigma^2}\left(\dfrac{q_k - a\rho}{a\rho}\right)^2\right)\Bigg|_{\rho_{c,l}}^{\rho_{c,u}} & a < a_k \\ -\exp\left(\dfrac{-1}{2\sigma^2}\left(\dfrac{a - Q_k\rho}{a}\right)^2\right)\Bigg|_{\rho_{c,l}}^{\rho_{c,u}} & a > a_k \,. \end{cases} \tag{18}$$

The majority of currently available exoplanet data for WFIRST-imageable planets has been obtained from radial velocity (RV) surveys. While transit photometry currently leads in the total number of exoplanet discoveries, most of these (primarily due to Kepler and the K2 mission) are too distant for imaging with the next generation of space-based coronagraphic instruments, and the WFIRST CGI in particular. While we expect this to change with TESS and other surveys, for now, the true mass m_k of the majority of known exoplanets of interest remains undetermined, while only the minimum mass $m_{k,min} = m_k \sin I$ is known. In these cases, we rewrite the probability integral (17) as $S_\rho(a, m, m_k)$ and we introduce the system's inclination $I \in [0, \pi)$ as a new random variable with a sinusoidal probability density function $f_{\bar{I}}(I) = I/2$. We can then take into account the effect of the known planet's mass uncertainty by using Equation (18) and defining

$$S'_\rho(a, m) = \int_0^\pi S_\rho \left(a, m, \frac{m_{k,min}}{\sin(I)} \right) f_{\bar{I}}(I) dI \,. \tag{19}$$

For the stability criteria based on ρ, Equations (18) and (19) will be directly used for the computation of analytic stability maps. Similarly, we now derive the equivalent formulation for the angular momentum deficit C.

3.2. *C Conditional Density Function*

For a two-planet system ($n_p = 2$), Equation (8) can be written as

$$C = g_C(e, a, m) = K + \Lambda(1 - \sqrt{1 - e^2}) \,, \tag{20}$$

where $K = \Lambda_k(1 - \sqrt{1 - e_k^2})$ accounts for the known planet AMD contribution. For fixed values of a and m, $\Lambda = m\sqrt{GM_\star a}$ is completely defined and therefore $C = g_C(e \mid a, m)$ is only a function of e. The inverse function $g_C^{-1}(C \mid a, m)$, which we will denote as h_C, is then obtained by solving Equation (20) for the eccentricity

$$e = h_C(C \mid a, m) = \sqrt{1 - \left(\frac{\Lambda - C + K}{\Lambda} \right)^2} \,, \tag{21}$$

where again the conditional notation will be dropped for simplicity. Since the inverse function must have the range $e = h_C(C) \in [0, 1)$, the derivative

$$\left| \frac{dh_C}{dC}(C) \right| = \frac{1}{\Lambda} \left(\frac{\sqrt{1 - h_C^2(C)}}{h_C(C)} \right) \tag{22}$$

is well defined except for the case $C = K$ (i.e. $h_C(C) = 0$). However, this singularity is naturally solved when the expression of the conditional density function is simplified

$$f_{\bar{C}|\bar{a},\bar{m}}(C \mid a, m) = f_{\bar{e}}(h_C(C)) \left| \frac{dh_C}{dC}(C) \right| = \frac{\sqrt{1 - h_C^2(C)}}{\Lambda \sigma^2} \exp \left(\frac{-h_C^2(C)}{2\sigma^2} \right) \,, \tag{23}$$

where the formula of the Rayleigh probability density function for $f_{\bar{e}}(e)$ has been used. Following the same procedure as in Section 3.1, for certain values of $C_{c,l}(a, m)$ and $C_{c,u}(a, m)$ determined by the specific AMD stability criterion used, the integral of the conditional density function is

$$S_C(a, m) = \int_{C_{c,l}}^{C_{c,u}} f_{\bar{C}|\bar{a},\bar{m}}(C \mid a, m) dC = F_{\bar{e}}(h_C(C_{c,u})) - F_{\bar{e}}(h_C(C_{c,l})) \,. \tag{24}$$

Making use of Equation (21), the analytic solution is then given by

$$S_C(a, m) = -\exp \left(\frac{1}{2\sigma^2} \left(\left(\frac{\Lambda - C + K}{\Lambda} \right)^2 - 1 \right) \right) \Bigg|_{C_{c,l}}^{C_{c,u}} \,. \tag{25}$$

As described in the previous subsection, in the case of systems with an undetermined planetary mass m_k, we redefine the probability of having a stable configuration as

$$S_C^{'}(a,m) = \int_0^{\pi} S_C\left(a, m, \frac{m_{k,min}}{\sin(I)}\right) f_{\bar{I}}(I) dI\,. \tag{26}$$

Although a more detailed and consistent single-planet ranking is described in Section 5, a first approach relies on the definition of the a, m and C (or ρ) joint probability density function

$$f_{\bar{a},\bar{m},\bar{C}}(a,m,C) = f_{\bar{a},\bar{m}}(a,m) \cdot f_{\bar{C}|\bar{a},\bar{m}}(C \mid a,m)\,. \tag{27}$$

By choosing the appropriate limits of integration which approximately define the imageable region, together with the stability boundaries of C, a rapid estimation of the probability of detecting a stable planet can be computed as

$$\int_{m_l}^{m_u} \int_{a_l}^{a_u} f_{\bar{a},\bar{m}}(a,m) \left(\int_{C_{c,l}}^{C_{c,u}} f_{\bar{C}|\bar{a},\bar{m}}(C \mid a,m)\, dC \right) da\, dm\,, \tag{28}$$

where the term in the inner parentheses has already been analytically solved, simplifying the calculation to a double integral. Equation (28), which can be equivalently derived for ρ, can be used to discard those systems with barely any stable imageable region or to obtain a first imaging prioritization in a fast and computationally inexpensive manner.

4. ANALYTIC STABILITY MAPS

Following the previous assumptions and derivations, in this section we compute the analytic stability maps which will allow us to rapidly characterize the stable region of a particular single-planet system. Essentially, these maps consist of a regular grid with 100 semi-major axis bins and 100 mass bins, both logarithmically spaced and ranged around the system's imageable region. For a particular pair (a, m), the value of the corresponding bin represents the probability of having a stable configuration according to the specific criterion used. For the systems where the known planet's mass m_k is completely determined, the stability maps are built using Equations (18) and (25), depending on the type of criterion used. On the other hand, if only $m_k \sin I$ is known, Equations (19) and (26) are employed. To illustrate this, we select the empirical criterion presented by Petrovich (2015), since it appears to give the most conservative and consistent boundaries according to the results from Section 2.3. Based on the critical ρ from inequality (7), we define the lower limit of integration

$$\rho_{c,l}^{\mathrm{P}}(a,m) = \begin{cases} 1.15 + 2.4\left[\max(\mu,\mu_k)^{1/3}\right]\left(a_k/a\right)^{1/2} & a < a_k \\ 1.15 + 2.4\left[\max(\mu_k,\mu)^{1/3}\right]\left(a/a_k\right)^{1/2} & a > a_k\,. \end{cases} \tag{29}$$

In general, given that we are only considering elliptical orbits (i.e $e \in [0,1)$), the outer pericenter to inner apocenter ratio must have a range $\rho \in (g_\rho(1,a), g_\rho(0,a)]$ and therefore, $\rho_{c,l}$ should always be conveniently adjusted to the range of values of ρ. That is, if $\rho_{c,l}(a,m) < g_\rho(1,a)$ then $\rho_{c,l}(a,m) = g_\rho(1,a)$, and equivalently if $\rho_{c,l}(a,m) > g_\rho(0,a)$ then $\rho_{c,l}(a,m) = g_\rho(0,a)$. Furthermore, the expression of $g_\rho(0,a)$ allows us to set the upper limit as

$$\rho_{c,u}(a) = g_\rho(0,a) = \begin{cases} \dfrac{q_k}{a} & a < a_k \\ \dfrac{a}{Q_k} & a > a_k\,. \end{cases} \tag{30}$$

In addition, we will also construct stability maps using Giuponne's criterion (Giuppone et al., 2013, Equation 6) and the Hill AMD criterion (Petit et al., 2018, Equation 12), which will serve as an alternative for ranking planetary systems. In the first case, the lower limit of integration is directly given by Equation (6) and can be written as

$$\rho_{c,l}^{\mathrm{G}}(a,m) = \begin{cases} \dfrac{1}{1 - 1.46\epsilon^{2/7}} & a < a_k \\ 1 + 1.46\epsilon^{2/7} & a > a_k\,, \end{cases} \tag{31}$$

while the upper limit $\rho_{c,u}$ is again given by Equation (30). On the other hand, assuming that the stellar mass $M_\star$ is known, the Hill critical AMD is only a function of the semi-major axis and mass ratios. From the definition of $C_c^{\mathrm{H}}(\alpha,\gamma)$ given in Equation (12), we then derive the upper limit of integration as

$$C_{c,u}(a,m) = \begin{cases} \Lambda_k\, C_c^{\mathrm{H}}(a/a_k, m/m_k) & a < a_k \\ \Lambda\, C_c^{\mathrm{H}}(a_k/a, m_k/m) & a > a_k\,, \end{cases} \tag{32}$$

for which again the range of values of $C \in [g_C(0,a,m), g_C(1,a,m))$ should be taken into consideration. In particular, the lower limit of integration is defined and given by $C_{c,l}(a,m) = g_C(0,a,m) = K$.

We demonstrate this procedure by generating the (a, m) analytic stability maps of the single-planet systems HD 154345 and HD 114613 (Figure 2). Since none of the system's inclinations are known, we make use of Equations (19) and (26), together with the limits of integration presented above. The mean eccentricity for the Rayleigh distribution is taken to be $\mu_e = 0.225$ (Moorhead et al., 2011) and the required orbital parameters, as well as the range of values of a and m, are as in Table 1. The code used to compute the analytic stability maps and perform the single-planet ranking presented in the following section, can be found at `https://github.com/CarlosGascon/StableDoS`.

Furthermore, we can easily build (a, R) stability maps by considering instead a set of logarithmically spaced planetary radius R bins and applying the previous expressions to the corresponding planetary masses. For each value of R, the related mass m is predicted using the FORECASTER best-fit density model (Chen and Kipping, 2016), originally composed of linear segments (in log-log space) of the form

$$R = 10^{C + \log_{10}(m) S}\,, \tag{33}$$

where C and S are fit coefficients defined in four mass intervals: Terran, Neptunian, Jovian and Stellar Worlds. Due to inclusion of many tidally locked, inflated Jupiters in the model, the original results tend to overestimate

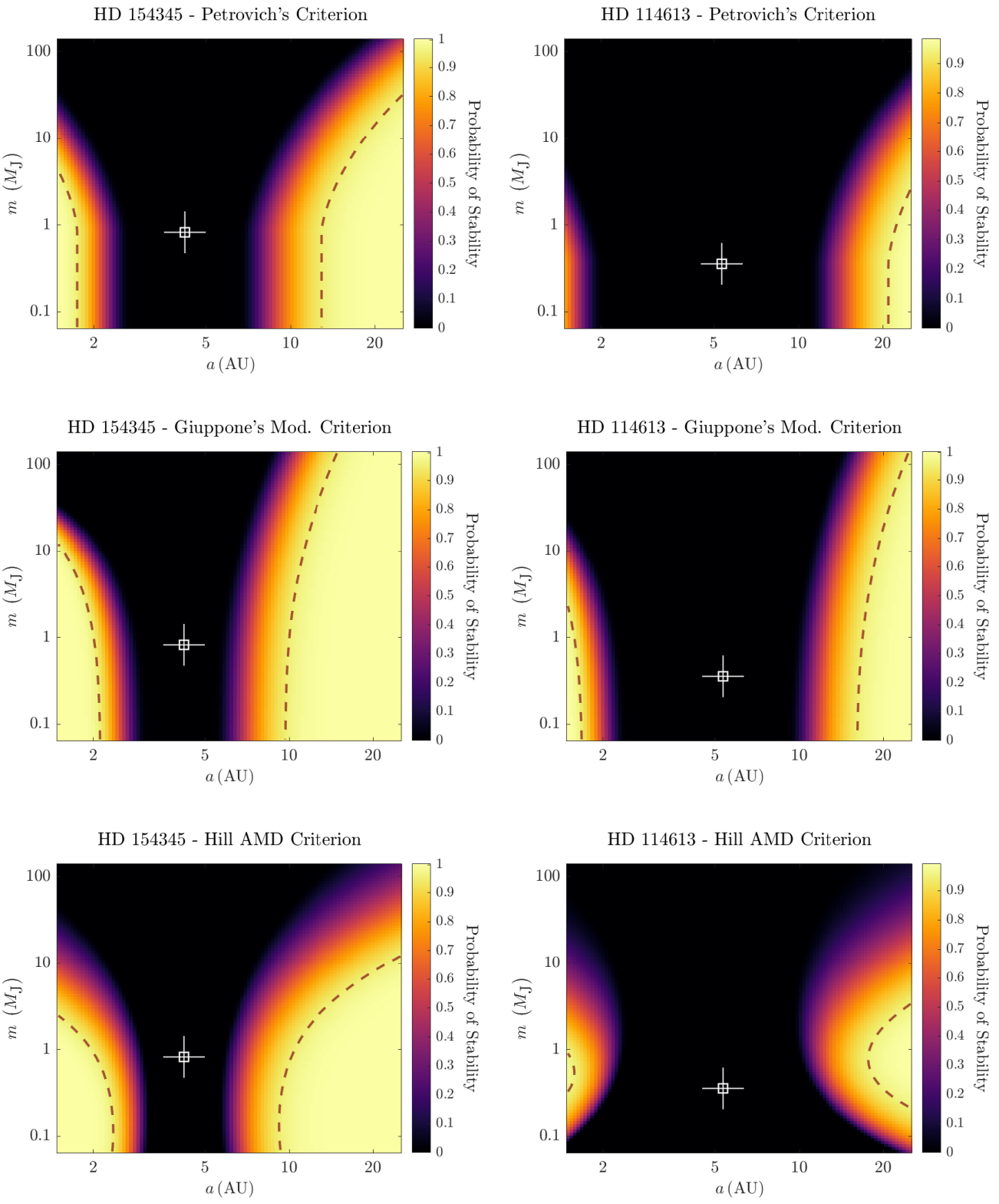

Figure 2. Analytic stability maps for the systems HD 154345 (left column) and HD 114613 (right column), using Petrovich's empirical criterion (top row), Giuppone's modified criterion (middle row) and the Hill AMD criterion (bottom row). The white marker indicates the position of the existing planet and the dashed curve accounts for the 0.95 contour line.

Table 2. C and S parameters of the FORECASTER modified fit

m ($M_\oplus$)	C	S
$m \leqslant 2.04$	0.00346053	0.279
$2.04 < m \leqslant 95.16$	-0.06613329	0.50376436
$95.16 < m \leqslant 317.828407$	0.48091861	0.22725968
$317.828407 < m \leqslant 26635.6863$	1.04956612	0
$m > 26635.6863$	-2.84926757	0.881

the radius for Jovian-size planets, and so we slightly modify the initial fit by moderating the transition between the Saturn and Jupiter mass-radius points. Specifically, the Neptunian Worlds segment is adjusted to end at the Saturn mass-radius point, from which a new fit is added as a straight line (in the log-log space) until the Jupiter mass-radius point. Moreover, the Jovian segment is corrected to be a constant Jupiter radius value ranging from 1 Jupiter Mass through 0.08 Solar Masses. The Terran and Stellar Worlds, on the other hand, remain unchanged. The resultant values of C and S, for Earth mass and radius units, are shown in Table 2.

It is important to note that we are not suggesting that our modified fit is in any way more 'correct' than the original FORECASTER model. Rather, as we are focusing on only the larger orbits amenable to direct imaging, we wish to avoid generating planetary mass objects of greater than 1 Jupiter radius, which are expected to be exceedingly rare at the relevant separations. As the original fit also passes quite near the Saturn mass-radius point, we chose to explicitly incorporate it in our modification as well.

5. SINGLE-PLANET SYSTEMS PRIORITIZATION

Having constructed the analytic stability maps, we now address the main purpose of this study by identifying which single-planet systems are more likely to host an additional, imageable planet. Basically, the proposed methodology consists of estimating and comparing the expected number of planets (i.e., occurrence rates) within each system's stable-imageable region defined in the (a, R) space. To do so, together with the stability maps obtained in Section 4, we shall make use of the following additional grids:

1. *Depth-of-search grid:* Given a particular system, we obtain its imageable region by computing the depth-of-search grids as defined by Garrett et al. (2017). For given values of a and R, the corresponding bin represents the conditional probability of detecting a hypothetically existing planet (i.e., completeness Brown (2005)) according to the considered instrument's design and capabilities. In particular, here we set the necessary optical parameters and contrast limits according to the WFIRST CGI's inner and outer working angles and predicted contrast curve in the 575 nm imaging band. For planet photometry, we use the model grids from Batalha et al. (2018), which are interpolated to find the phase curves of various planets in reflected light.

2. *Occurrence grid:* In order to calculate the expected number of planets in a certain region, we build occurrence grids using the SAG 13 parametric fit for G-dwarfs. Similarly to Garrett and Savransky (2018), we translate the original period-radius broken power law into the (a, R) space and we add an exponential decay term starting at $a_k = 10$ AU.

Given that the size of the imageable region strongly depends on the distance from the observer to the target star, all three grids are ranged according to each system's detection boundaries ($a_{\min}$, $a_{\max}$ and $R_{\min}$). This is intended to increase the accuracy of the results by only calculating stability around the imageable zone. In general, the maximum planetary radius is set to $R_{\max} = 17R_{\oplus}$, since we only wish to consider bodies near the planetary mass regime. For the semi-major axis, the inner limit will be essentially determined by the minimum projected separation

$$a_{\min} = s_{\min} = IWA \cdot d\,, \tag{34}$$

where IWA is the telescope's inner working angle and d is the distance to the system. To find the maximum value of a, we consider the expression for the ratio of fluxes between the planet and the star (Brown, 2005)

$$F_R = p\Phi\left(\beta\right)\left(\frac{R}{r}\right)^2\,, \tag{35}$$

where p and β are the planet's albedo and phase angle respectively, Φ is the phase function and r is the distance between the planet and the star. For a particular value of R, the upper limit of the imageable region is characterized by the maximum a such that the planet meets the instrument's obscurational and photometric contraints, determined by $s_{\min}$ and the expected mininum contrast $c_{\min}$. These values can be related to the upper boundary of the nonzero region of the completeness joint probability density function (Garrett and Savransky, 2016) given by one of the solutions of

$$F(a \mid R) = c_{\min} - p\Phi\left[\sin^{-1}\left(\frac{s_{\min}}{a}\right)\right]\left(\frac{R}{a}\right)^2 = 0\,, \tag{36}$$

where r has been replaced by a, since the depth-of-search grids are defined assuming that $e = 0$ (Garrett et al., 2017). Since the width of the imageable region increases with R, the maximum semi-major axis $a_{\max}$ is consequently given by the upper bounding solution of the equation $F(a \mid R_{\max}) = 0$, where again $R_{\max}$ is the largest planetary radius considered. Having determined $a_{\min}$ and $a_{\max}$, we can finally obtain the minimum radius by isolating R in Equation (36) and calculating

$$R_{\min} = \min_{a\in(a_{\min},a_{\max})}\left\{\sqrt{\frac{a^2 c_{\min}}{p\Phi\left(\sin^{-1}\left(s_{\min}/a\right)\right)}}\right\}\,. \tag{37}$$

For each system, the product of the stability and depth-of-search grids yields the intersection between the stable and imageable regions, where the value of each bin gives the probability of detecting a stable planet of radius R and semi-major axis a. For instance, in Figure 3 we represent the resultant grids for the systems HD 154345 and HD 114613, using the Hill AMD and Petrovich's criteria respectively. In order to properly identify the limits of the nonzero regions, the bins with null probability are not coloured. As expected, in both cases the size of the imageable region is clearly defined by the solutions to the equations presented above. Such limits, together with the estimated detection probability of each bin, are only a function of the distance to the system and the instrument's capabilities. In consequence, the resemblance between both depth-of-search grids can be directly related to the similar target distance (see Table 1), while also evidencing that the results ignore integration time constraints since there is no dependence on the magnitude of the star.

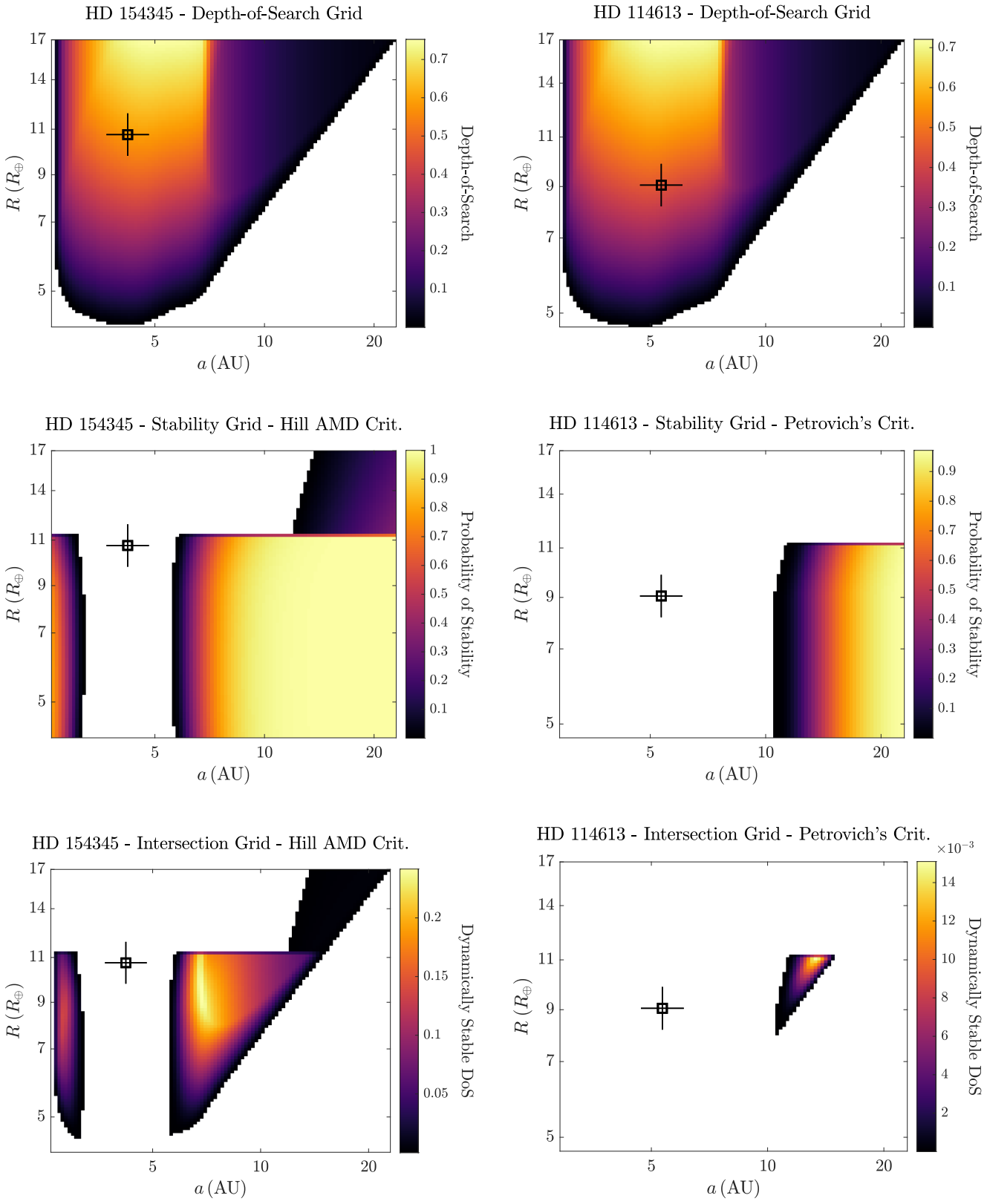

Figure 3. Depth-of-Search (top), Stability (middle) and Intersection (bottom) grids for the system HD 154345 using the Hill AMD criterion (left), and the system HD 114613 using Petrovich's criterion (right). The black marker indicates the position of the existing planet.

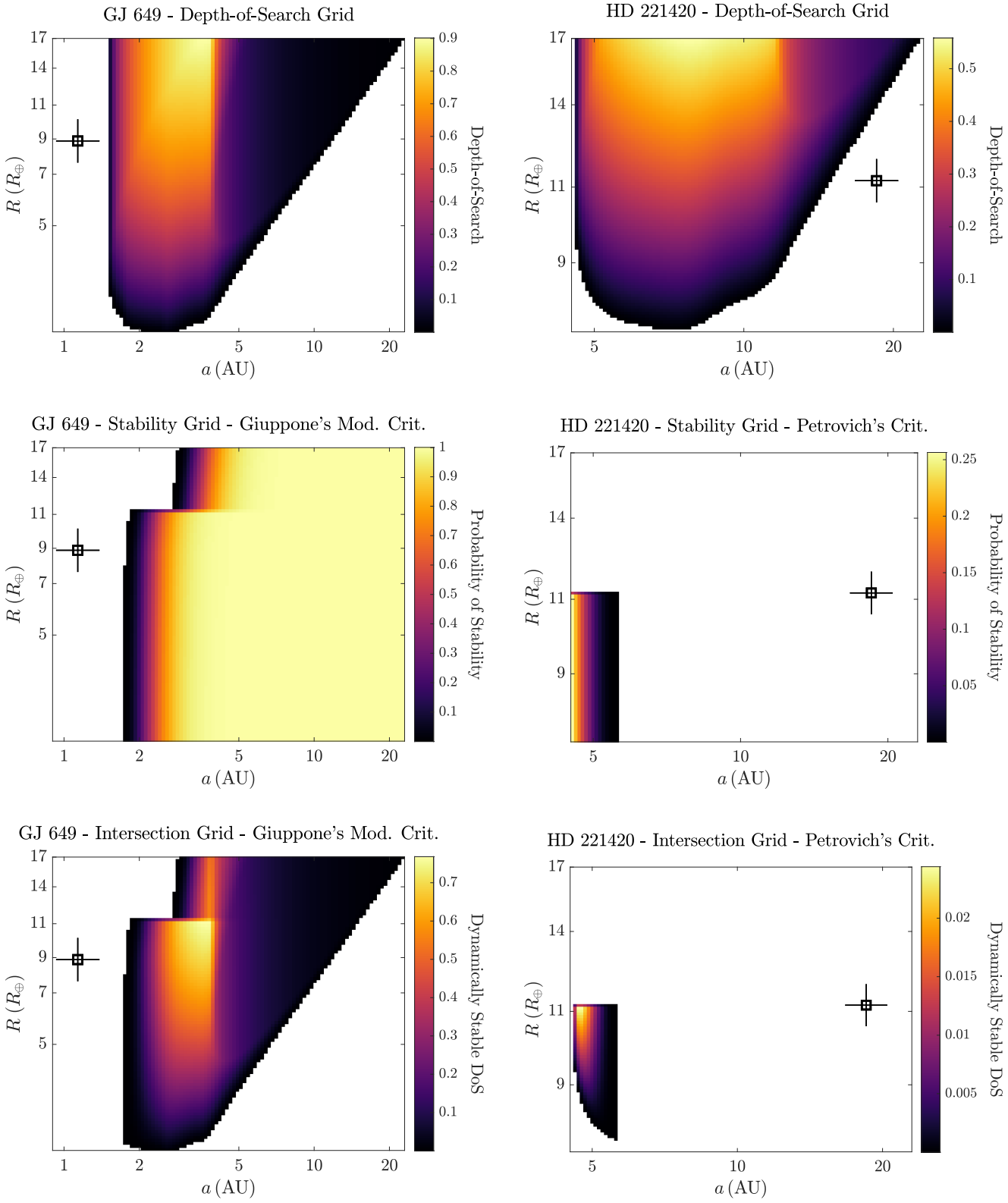

Figure 4. Depth-of-Search (top), Stability (middle) and Intersection (bottom) grids for the system GJ 649 using Giuppone's modified criterion (left), and the system HD 221420 using Petrovich's criterion (right). The black marker indicates the position of the existing planet.

Regarding the (a, R) stability maps, we first note a clear contrast between the extension of the unstable regions of both systems, essentially as a result of the difference in the orbital eccentricities of the existing planets and the stability criteria employed. Moreover, the use of the modified FORECASTER best-fit described in Section 4 results in a discontinuous increase in planetary mass occurring at 1 $R_{\rm J}$ ($\approx 11.2 R_{\oplus}$), causing the steep growth in the unstable region observed at that point.

In general, the stable-imageable grid demonstrates how the depth-of-search is highly perturbed by the region where planets cannot exist due to instabilities, confirming that the presence of the known planet should be considered when optimizing the target selection. The sum over the intersection bins, normalized by the number of bins and multiplied by the grid area, yields what we refer to as the dynamically stable depth-of-search. This value has no dependence on the assumed planet population and only accounts for the considered instrument's performance and stability criterion. Finally, the convolution of the intersection region with the occurrence grid returns the desired estimation of the expected number of stable and imageable planets in the system (i.e., dynamically stable completeness), obtaining a metric that can be directly compared for imaging prioritization. We apply this procedure to 189 currently known single-planet systems within a distance of 50 pc, creating a ranking based on Petrovich's stability criterion and complemented by the results obtained with the Hill AMD and Giuppone's criteria (Appendix A). Naturally, the results show a clear dependence on the system's distance d, generally being the closest targets the most valuable. Nonetheless, we also note how some of the nearest stars present a lower dynamically stable completeness in comparison to farther targets with smaller imageable regions. Although we are focusing on the search of unknown companions, the systems where the already existing exoplanet falls inside the detectable region (such as HD 154345 or HD 114613) are in any case interesting targets, given that the majority of known exoplanets have been discovered with indirect detection techniques and still need to be directly imaged. Alternatively, in Figure 4 we represent the resultant grids for the systems GJ 649 and HD 221420, where the existing planet is located outside the lower and upper limits of the imageable region respectively.

6. CONCLUSIONS

Running numerical simulations up to 10^9 years, we have analyzed and compared various stability criteria for two-planet systems with arbitrary eccentricities, showing that the criterion from Petrovich (2015) is generally the most conservative and convenient, while the stability limits defined by Giuppone et al. (2013) and Petit et al. (2018) also perform reasonably well. For any criterion expressed as a boundary of the outer pericenter to inner apocenter ratio (ρ) or the angular momentum deficit (C), we have derived expressions for the conditional probability of having a stable companion given fixed values of a and m. This formulation has been directly used for the computation of analytic stability maps, allowing us to rapidly characterize the stable region of a system in the (a, R) space. By intersecting with the depth-of-search grids defined by Garrett et al. (2017), we have obtained the corresponding stable-imageable region, yielding the definition of the total dynamically stable depth-of-search, with no dependence on the assumed planet population. In particular, we have presented two cases where the detectable region is clearly perturbed by the stability boundaries, remarking the importance of accounting for the effects of the existing planet in such systems. Furthermore, we added two examples of systems where the existing planet falls outside the imageable region but its gravitational effect is still noticeable. Finally, the convolution with the selected occurrence grid returns the expected number of stable and imageable planets in the system.

Applying this procedure to 189 currently known single-planet systems and several stability criteria, we have built a ranked target list based on the WFIRST CGI's capabilities and the SAG13 parametric fit. The code used for both the numerical simulations and the construction of analytic stability maps is publicly available at `https://github.com/CarlosGascon`. Although a numerical analysis could lead to more accurate results, the proposed methodology is a powerful tool, not only for rapidly identifying which targets have a higher probability of hosting an additional planet, but also for discarding those systems where no unknown companions can be detected.

7. ACKNOWLEDGEMENTS

This research made use of the NASA Exoplanet Archive, which is operated by the California Institute of Technology, under contract with the National Aeronautics and Space Administration under the Exoplanet Exploration Program. In addition, this research employed the Imaging Mission Database, which is operated by the Space Imaging and Optical Systems Lab (SIOSlab) at Cornell University, where this work was developed. Especially, I would like to express my gratitude to my advisor Dmitry Savransky, whose guidance and continuous support was essential for the completion of this project. Finally, I would also like to thank the Interdisciplinary Higher Education Center (CFIS) from the Polytechnic University of Catalonia (UPC), as well as the CELLEX Foundation, for offering me the opportunity of developing this work at Cornell University.

REFERENCES

Agnew, M. T., Maddison, S. T., and Horner, J. (2018). Prospecting for exo-earths in multiple planet systems with a gas giant. *Monthly Notices of the Royal Astronomical Society*, 481(4):4680–4697.

Batalha, N. E., Smith, A. J., Lewis, N. K., Marley, M. S., Fortney, J. J., and Macintosh, B. (2018). Color classification of extrasolar giant planets: Prospects and cautions. *The Astronomical Journal*, 156(4):158.

Brown, R. A. (2005). Single-visit photometric and obscurational completeness. *The Astrophysical Journal*, 624(2):1010.

Chen, J. and Kipping, D. (2016). Probabilistic forecasting of the masses and radii of other worlds. *The Astrophysical Journal*, 834(1):17.

Deck, K. M., Payne, M., and Holman, M. J. (2013). First-order resonance overlap and the stability of close two-planet systems. *The Astrophysical Journal*, 774(2):129.

Duncan, M., Quinn, T., and Tremaine, S. (1989). The long-term evolution of orbits in the solar system: A mapping approach. *Icarus*, 82(2):402–418.

Garrett, D. and Savransky, D. (2016). Analytical formulation of the single-visit completeness joint probability density function. *The Astrophysical Journal*, 828(1):20.

Garrett, D. and Savransky, D. (2018). Building better planet populations for exosims. In *American Astronomical Society, AAS Meeting*, volume 231.

Garrett, D., Savransky, D., and Macintosh, B. (2017). A simple depth-of-search metric for exoplanet imaging surveys. *The Astronomical Journal*, 154(2):47.

Giuppone, C., Morais, M., and Correia, A. (2013). A semi-empirical stability criterion for real planetary systems with eccentric orbits. *Monthly Notices of the Royal Astronomical Society*, 436(4):3547–3556.

Gladman, B. (1993). Dynamics of systems of two close planets. *Icarus*, 106(1):247–263.

Hadden, S. and Lithwick, Y. (2018). A criterion for the onset of chaos in systems of two eccentric planets. *The Astronomical Journal*, 156(3):95.

Konopacky, Q. M., Barman, T. S., Macintosh, B. A., and Marois, C. (2013). Detection of carbon monoxide and water absorption lines in an exoplanet atmosphere. *Science*, 339(6126):1398–1401.

Laskar, J. (2000). On the spacing of planetary systems. *Physical Review Letters*, 84(15):3240.

Laskar, J. and Petit, A. (2017). Amd-stability and the classification of planetary systems. *Astronomy & Astrophysics*, 605:A72.

Marchal, C. and Bozis, G. (1982). Hill stability and distance curves for the general three-body problem. *Celestial Mechanics*, 26(3):311–333.

Moorhead, A. V., Ford, E. B., Morehead, R. C., Rowe, J., Borucki, W. J., Batalha, N. M., Bryson, S. T., Caldwell, D. A., Fabrycky, D. C., Gautier III, T. N., et al. (2011). The distribution of transit durations for kepler planet candidates and implications for their orbital eccentricities. *The Astrophysical Journal Supplement Series*, 197(1):1.

Petit, A. C., Laskar, J., and Boué, G. (2017). Amd-stability in the presence of first-order mean motion resonances. *Astronomy & Astrophysics*, 607:A35.

Petit, A. C., Laskar, J., and Boué, G. (2018). Hill stability in the amd framework. *Astronomy & Astrophysics*, 617:A93.

Petrovich, C. (2015). The stability and fates of hierarchical two-planets systems. *The Astrophysical Journal*, 808(2):120.

Rein, H. and Liu, S.-F. (2012). Rebound: an open-source multi-purpose n-body code for collisional dynamics. *Astronomy & Astrophysics*, 537:A128.

Wisdom, J. (1980). The resonance overlap criterion and the onset of stochastic behavior in the restricted three-body problem. *The Astronomical Journal*, 85:1122–1133.

A. SINGLE-PLANET SYSTEMS RANKING

Table 3. Dynamically stable depth-of-search and completeness values obtained using Petrovich's, Giuppone's, and the Hill AMD criteria. The results are ranked according to the completeness values calculated with Petrovich's criterion.

Target		Petrovich's Crit.		Giuppone's Crit.		Hill AMD Crit.	
Name	Distance (pc)	DoS (Dynamically Stable)	Completeness (Dynamically Stable)	DoS (Dynamically Stable)	Completeness (Dynamically Stable)	DoS (Dynamically Stable)	Completeness (Dynamically Stable)
Proxima Cen	1.29	44.24	0.40551	52.07	0.41417	39.36	0.39529
GJ 411	2.55	52.74	0.36635	57.83	0.37178	45.10	0.35241
Ross 128	3.38	56.36	0.36253	57.89	0.36422	44.39	0.34085
GJ 674	4.55	59.15	0.35824	59.22	0.35833	48.65	0.33922
GJ 687	4.55	54.38	0.35171	59.20	0.35829	46.51	0.33472
GJ 625	6.49	61.57	0.33250	61.90	0.33296	46.37	0.30134
HD 180617	5.91	47.38	0.31862	59.09	0.34147	44.13	0.30938
Gl 686	8.16	62.30	0.30438	62.40	0.30452	45.93	0.27003
GJ 433	9.07	61.39	0.28633	61.40	0.28633	46.16	0.25442
HD 285968	9.47	60.72	0.27940	60.73	0.27941	45.44	0.24688
GJ 436	9.76	61.41	0.27324	61.41	0.27324	53.47	0.25771
GJ 1265	10.26	61.33	0.26413	61.33	0.26413	49.17	0.23932
GJ 536	10.41	61.58	0.26188	61.59	0.26189	44.50	0.22627
GJ 86	10.79	60.60	0.25471	60.61	0.25473	60.58	0.25467
HD 102365	9.29	46.68	0.25305	60.46	0.28073	42.19	0.24034
HD 147379	10.77	57.22	0.24945	60.68	0.25505	42.52	0.21667
HD 85512	11.28	56.84	0.24178	59.67	0.24641	37.89	0.19852
HD 3651	11.14	49.03	0.22822	60.18	0.24871	42.86	0.19890
GJ 96	11.94	51.28	0.22096	59.49	0.23535	40.26	0.19454
HD 211970	13	58.40	0.21789	58.48	0.21803	40.11	0.17966
GJ 685	14.32	56.90	0.19775	56.92	0.19778	37.47	0.15785
Gl 378	14.96	56.53	0.18868	56.53	0.18869	45.72	0.16748
51 Peg	15.47	55.16	0.18147	55.16	0.18147	54.73	0.18073
HIP 79431	14.54	47.86	0.17898	56.73	0.19474	50.32	0.17229
tau Boo	15.66	55.17	0.17870	55.17	0.17870	55.17	0.17870
HD 177565	16.93	53.47	0.16163	53.54	0.16175	32.81	0.12110
GJ 3942	16.94	53.50	0.16162	53.51	0.16162	36.18	0.12781
HD 99492	18.21	51.17	0.14590	51.21	0.14596	36.71	0.11838
70 Vir	17.91	45.37	0.13814	51.75	0.14952	31.18	0.06765
GJ 3021	17.56	41.02	0.13318	52.29	0.15379	31.72	0.07319
HR 810	17.33	39.74	0.13230	52.05	0.15566	40.97	0.13318
HD 192263	19.65	49.38	0.12921	49.39	0.12923	47.07	0.12521
HD 104067	20.38	48.34	0.12136	48.41	0.12147	33.61	0.09494
GJ 649	10.38	19.02	0.11644	33.36	0.17733	22.72	0.12031
HD 27442	18.28	33.25	0.10883	49.18	0.14084	33.70	0.11120
HD 90156	21.96	45.78	0.10545	45.96	0.10574	25.81	0.07127
HD 4308	22.03	45.71	0.10502	45.71	0.10502	29.52	0.07730

Table 3 continued on next page

Table 3. *(continued)*

Target		Petrovich's Crit.		Giuppone's Crit.		Hill AMD Crit.	
Name	Distance	DoS	Completeness	DoS	Completeness	DoS	Completeness
	(pc)	(Dynamically Stable)		(Dynamically Stable)		(Dynamically Stable)	
HD 147513	12.91	18.76	0.09718	36.59	0.16009	17.02	0.07226
HD 39855	23.28	43.83	0.09364	43.83	0.09364	31.51	0.07335
HIP 12961	23.39	43.40	0.09253	43.49	0.09267	36.14	0.08056
HD 62509	10.34	14.14	0.08778	27.77	0.14964	23.74	0.14113
alf Ari	20.21	29.00	0.08573	46.18	0.11943	30.00	0.08271
HD 156668	24.35	41.73	0.08465	41.73	0.08465	23.43	0.05555
HD 42618	24.35	40.24	0.08235	41.72	0.08465	18.04	0.04719
HD 19994	22.54	31.68	0.07736	44.25	0.09911	28.41	0.07206
HD 16417	25.41	40.37	0.07640	40.37	0.07641	26.16	0.05467
alf Tau	20.43	23.15	0.06803	43.99	0.11322	31.01	0.08361
HD 103949	26.52	37.91	0.06749	38.51	0.06837	15.19	0.03489
HD 33564	20.97	23.40	0.06584	45.14	0.11157	22.30	0.04140
HD 210277	21.31	21.54	0.06324	42.74	0.10522	20.85	0.04918
HD 179949	27.48	37.02	0.06204	37.02	0.06204	37.01	0.06204
gam Cep	13.54	11.61	0.05853	24.50	0.11021	19.57	0.09668
HD 125595	28.22	35.59	0.05742	35.59	0.05742	18.00	0.03347
HD 164595	28.28	35.64	0.05703	35.65	0.05704	16.88	0.03169
HD 10647	17.34	14.42	0.05688	29.20	0.10051	19.64	0.07528
HD 93083	28.54	34.76	0.05475	35.31	0.05554	23.91	0.03983
HD 75289	29.14	34.48	0.05209	34.48	0.05209	34.42	0.05201
HD 21411	29.16	34.02	0.05140	34.43	0.05199	21.71	0.03514
HD 102195	29.36	33.97	0.05095	33.97	0.05095	33.87	0.05082
HD 46375	29.58	33.59	0.04972	33.59	0.04972	33.31	0.04934
HD 101930	30.05	32.87	0.04722	32.94	0.04731	23.62	0.03523
HD 52265	30.01	32.52	0.04680	33.04	0.04751	29.55	0.04280
HD 218566	28.85	29.71	0.04652	34.74	0.05377	16.39	0.02947
7 CMa	19.82	13.83	0.04466	31.95	0.09044	15.10	0.04114
HD 162020	30.85	31.45	0.04335	31.45	0.04335	31.40	0.04323
HD 8326	30.71	31.05	0.04302	31.78	0.04402	16.66	0.02535
HD 128356	26.03	19.20	0.04014	38.84	0.07121	24.49	0.04687
HD 64114	31.55	30.40	0.04010	30.41	0.04011	13.45	0.02018
HD 130322	31.91	29.96	0.03848	29.96	0.03849	29.94	0.03846
HIP 71135	32.36	28.97	0.03642	29.08	0.03656	11.29	0.01656
HIP 35173	33.19	27.96	0.03323	27.97	0.03324	10.98	0.01492
HD 22781	32.63	26.46	0.03229	28.86	0.03546	23.83	0.02921
HD 106515 A	34.12	24.81	0.02776	26.47	0.02987	25.50	0.02860
HD 45652	34.89	25.25	0.02719	25.32	0.02727	22.60	0.02420
HD 63765	32.57	20.78	0.02495	28.98	0.03568	15.32	0.01992
BD-11 4672	27.3	11.50	0.02437	28.83	0.04993	12.47	0.02798
16 Cyg B	21.15	7.42	0.02279	24.29	0.06416	5.32	0.00864

Table 3 continued on next page

Table 3. *(continued)*

Target		Petrovich's Crit.		Giuppone's Crit.		Hill AMD Crit.	
Name	Distance	DoS	Completeness	DoS	Completeness	DoS	Completeness
	(pc)	(Dynamically Stable)		(Dynamically Stable)		(Dynamically Stable)	
HD 114386	27.95	11.40	0.02257	31.48	0.05175	15.47	0.02921
HD 216770	36.7	22.17	0.02131	22.65	0.02187	17.88	0.01697
HD 195019	37.71	21.21	0.01928	21.21	0.01928	21.21	0.01928
HD 63454	37.73	21.17	0.01923	21.17	0.01923	21.08	0.01913
HD 117618	37.82	20.98	0.01899	20.99	0.01899	16.14	0.01435
HD 16141	37.83	20.94	0.01894	20.97	0.01897	14.03	0.01245
HD 23079	33.49	16.93	0.01857	27.25	0.03182	18.24	0.02107
HD 113337	36.22	18.69	0.01768	23.32	0.02320	20.99	0.02042
HD 108147	38.96	19.41	0.01644	19.41	0.01644	18.52	0.01555
HD 4208	34.23	15.63	0.01621	26.02	0.02920	10.63	0.01259
HD 102117	39.62	18.57	0.01508	18.57	0.01508	15.11	0.01198
HD 216437	26.71	6.99	0.01477	23.64	0.04185	10.05	0.01748
GJ 849	8.8	2.11	0.01471	6.50	0.04151	8.12	0.04800
HD 28185	39.43	17.99	0.01448	18.89	0.01545	18.25	0.01479
gam 1 Leo	38.52	17.33	0.01444	19.94	0.01736	19.32	0.01667
HD 114762	40.23	17.67	0.01383	17.74	0.01391	17.70	0.01385
HD 38283	38.1	16.16	0.01336	20.61	0.01833	8.86	0.00779
HD 111232	28.98	8.22	0.01310	28.52	0.04389	15.47	0.02011
HD 142415	35.57	13.80	0.01267	24.28	0.02504	18.23	0.01823
HD 83443	40.95	16.85	0.01262	16.85	0.01262	16.83	0.01260
HD 178911 B	41.02	16.73	0.01250	16.73	0.01251	16.73	0.01250
HD 98736	32.48	9.50	0.01185	26.57	0.03297	14.83	0.01852
kap CrB	30.09	7.71	0.01173	23.10	0.03222	11.21	0.01781
HD 89744	38.68	14.95	0.01162	19.88	0.01700	18.03	0.01450
HD 103720	41.6	16.08	0.01155	16.08	0.01155	16.08	0.01155
HD 168746	41.62	16.05	0.01152	16.05	0.01152	15.80	0.01130
bet UMi	38.78	14.86	0.01150	19.69	0.01677	17.96	0.01493
HD 7199	36.19	13.18	0.01150	23.30	0.02319	6.45	0.00719
HD 121504	41.71	15.91	0.01138	15.91	0.01138	15.68	0.01117
HD 10697	33.15	10.23	0.01093	25.67	0.03040	16.88	0.01920
HD 197037	33	8.94	0.01080	25.08	0.02974	9.39	0.01283
HD 216435	33.01	9.25	0.01066	23.86	0.02803	9.01	0.01218
HD 6434	42.41	15.02	0.01032	15.02	0.01032	14.70	0.01004
HD 204941	28.74	4.85	0.01019	16.90	0.02533	7.83	0.01659
GJ 179	12.36	1.91	0.01012	6.68	0.03543	3.79	0.01857
HD 85390	33.56	8.02	0.00977	26.30	0.03050	6.17	0.00961
HD 70642	29.3	5.69	0.00972	19.99	0.02877	9.03	0.01691
HD 141937	33.39	9.36	0.00968	26.46	0.03103	19.30	0.01923
HD 49674	43.09	14.26	0.00937	14.26	0.00937	12.92	0.00831
HD 137388	40.53	12.99	0.00897	17.31	0.01333	5.15	0.00386

Table 3 continued on next page

Table 3. *(continued)*

Target		Petrovich's Crit.		Giuppone's Crit.		Hill AMD Crit.	
Name	Distance	DoS	Completeness	DoS	Completeness	DoS	Completeness
	(pc)	(Dynamically Stable)		(Dynamically Stable)		(Dynamically Stable)	
iot Dra	31.67	6.88	0.00875	28.08	0.03664	20.21	0.02218
HD 208487	44	13.22	0.00815	13.27	0.00820	9.87	0.00576
91 Aqr	44.08	13.14	0.00808	13.17	0.00811	12.87	0.00786
HD 42012	36.84	9.14	0.00713	22.01	0.02103	11.52	0.01047
HD 285507	45.09	12.10	0.00699	12.10	0.00699	12.10	0.00699
HD 8574	44.88	12.03	0.00697	12.31	0.00721	11.43	0.00653
30 Ari B	44.71	12.03	0.00695	12.52	0.00739	12.48	0.00735
HD 330075	45.36	11.82	0.00670	11.82	0.00670	11.82	0.00670
HIP 91258	45.95	11.20	0.00612	11.20	0.00612	11.19	0.00612
HD 77338	46	11.14	0.00608	11.14	0.00608	8.94	0.00467
HD 114729	37.85	7.82	0.00538	20.03	0.01784	7.32	0.00631
HD 17674	44.48	9.88	0.00522	12.69	0.00765	6.04	0.00315
HD 29021	31.02	3.11	0.00520	18.49	0.02331	6.62	0.00589
BD-17 63	34.49	3.36	0.00519	23.80	0.02593	12.96	0.01147
HD 164604	39.41	8.11	0.00495	18.73	0.01537	13.07	0.01004
HD 210193	42.25	9.01	0.00482	15.22	0.01051	4.77	0.00295
HD 30562	26.18	2.37	0.00481	12.23	0.02055	2.36	0.00212
mu Leo	32.63	3.96	0.00448	26.96	0.03281	20.08	0.02078
HD 154345	18.29	1.43	0.00422	5.19	0.01520	4.90	0.01734
HD 20782	36.02	3.34	0.00400	21.24	0.02064	10.46	0.00810
HD 143105	48.7	8.63	0.00394	8.63	0.00394	8.63	0.00394
HD 89307	32.04	2.67	0.00372	14.66	0.01594	5.71	0.00698
HD 107148	49.49	8.01	0.00344	8.01	0.00344	5.78	0.00232
HD 196885	34.2	2.62	0.00329	17.06	0.01705	7.33	0.00540
HD 167042	49.73	7.46	0.00307	7.81	0.00330	5.83	0.00225
BD+14 4559	49.42	7.15	0.00288	8.07	0.00348	6.37	0.00256
HD 50554	31.19	1.96	0.00282	16.92	0.02023	7.51	0.00590
HD 81040	34.47	2.70	0.00280	20.04	0.02079	12.88	0.01059
eps Tau	49.23	6.88	0.00270	8.17	0.00359	7.47	0.00315
HD 153950	48.52	6.83	0.00268	8.81	0.00406	7.65	0.00334
HD 117207	32.38	1.83	0.00258	11.42	0.01128	4.33	0.00619
HD 100777	49.6	6.41	0.00241	7.90	0.00338	5.47	0.00212
HD 213240	40.92	4.85	0.00213	16.15	0.01186	12.59	0.00833
HD 32963	38.12	2.15	0.00202	13.39	0.00984	2.55	0.00270
14 Her	17.94	0.55	0.00135	5.32	0.01546	0.79	0.00067
HD 222582	42.21	3.37	0.00117	15.06	0.01033	13.87	0.00911
HD 156846	47.8	3.92	0.00102	9.42	0.00455	9.32	0.00448
HD 4113	41.92	1.93	0.00081	15.16	0.01060	9.60	0.00587
HD 7449	38.71	0.66	0.00074	8.75	0.00493	1.64	0.00072
HD 70573	45.7	2.90	0.00062	11.27	0.00620	9.57	0.00490

Table 3 continued on next page

Table 3. *(continued)*

Target		Petrovich's Crit.		Giuppone's Crit.		Hill AMD Crit.	
Name	Distance	DoS	Completeness	DoS	Completeness	DoS	Completeness
	(pc)	(Dynamically Stable)		(Dynamically Stable)		(Dynamically Stable)	
eps Eri	3.21	0.09	0.00046	6.99	0.04011	0.13	0.00016
HD 106252	38.23	0.51	0.00044	11.97	0.00812	7.10	0.00349
HD 142022 A	34.31	0.43	0.00044	9.26	0.00698	3.68	0.00157
HD 171238	44.87	1.29	0.00021	10.99	0.00598	4.63	0.00184
HD 86226	45.74	1.52	0.00020	10.20	0.00524	1.80	0.00059
HD 187085	45.96	1.50	0.00020	10.57	0.00557	3.04	0.00127
HD 87883	18.3	0.12	0.00019	1.56	0.00299	0.16	0.00008
psi 1 Dra B	22.16	0.13	0.00016	1.67	0.00216	0.26	0.00017
HD 20868	47.79	1.34	0.00015	9.44	0.00457	6.89	0.00303
HD 221420	31.17	0.04	0.00009	1.11	0.00239	0.23	0.00034
GJ 328	20.54	0.03	0.00003	0.98	0.00120	0.08	0.00003
HD 220689	46.94	0.44	0.00002	7.78	0.00320	1.09	0.00023
HD 114613	20.29	0.02	0.00002	0.35	0.00031	0.14	0.00016
HD 45350	46.94	0.15	0.00001	8.99	0.00417	4.84	0.00191
HD 8673	37.9	0.01	0.00001	5.99	0.00252	4.66	0.00143
HD 24040	46.68	0.05	0.00000	4.52	0.00110	0.46	0.00003
HD 13931	47.46	0.07	0.00000	4.31	0.00099	0.29	0.00001
HD 108341	49.4	0.01	0.00000	6.66	0.00246	4.66	0.00152
HD 79498	49.02	0.00	0.00000	4.93	0.00134	1.46	0.00031
HD 40979	34.12	0.00	0.00000	0.78	0.00014	0.26	0.00001
HD 133131 B	47	0.00	0.00000	0.00	0.00000	0.00	0.00000
HD 13724	43.52	0.00	0.00000	0.06	0.00001	0.00	0.00000
HD 150706	28.29	0.00	0.00000	0.00	0.00000	0.00	0.00000
HD 166724	45.19	0.00	0.00000	0.13	0.00001	0.00	0.00000
HD 181234	47.81	0.00	0.00000	0.33	0.00002	0.00	0.00000
HD 196067	39.98	0.00	0.00000	0.00	0.00000	0.18	0.00000
HD 219077	29.21	0.00	0.00000	0.00	0.00000	0.00	0.00000
HD 220773	49	0.00	0.00000	0.00	0.00000	0.14	0.00000
HD 25015	37.47	0.00	0.00000	0.03	0.00000	0.00	0.00000
HD 92987	43.59	0.00	0.00000	0.02	0.00000	0.00	0.00000
HD 98649	42.22	0.00	0.00000	0.00	0.00000	0.00	0.00000
HIP 70849	24.07	0.00	0.00000	0.85	0.00003	0.00	0.00000